Ocean Engineering 60 (2013) 163–174

Contents lists available at SciVerse ScienceDirect

Ocean Engineering

journal homepage: www.elsevier.com/locate/oceaneng

Blade loads on tidal turbines in planar oscillatory flow

I.A. Milne [a,*], A.H. Day [b], R.N. Sharma [a], R.G.J. Flay [a]

[a] Department of Mechanical Engineering, The University of Auckland, Private Bag 92019, Auckland Mail Centre, Auckland 1142, New Zealand
[b] Department of Naval Architecture and Marine Engineering, University of Strathclyde, Henry Dyer Building, 100 Montrose Street, Glasgow G4 0LZ, UK

ARTICLE INFO

Article history:
Received 4 February 2012
Accepted 2 December 2012
Available online 26 January 2013

Keywords:
Tidal turbine
Unsteady hydrodynamics
Dynamic stall
Added mass
Rotor aerodynamics

ABSTRACT

Characterisation of the unsteady hydrodynamic loads is essential for accurate predictions of the fatigue life and ultimate loads of tidal turbine blades. This paper analyses a set of experimental tests of the hydrodynamic blade root out-of-plane bending moment response to planar oscillatory motion, chosen as an idealised representation of the unsteadiness imparted by waves and turbulence. Phenomena associated with dynamic stall are observed which are sensitive to the oscillatory frequency and velocity amplitude. Flow separation is shown to result in loads significantly greater in magnitude than that for steady flow. Following flow reattachment, the load cycles compare relatively well with Theodorsen's theory for a two-dimensional foil oscillating in heave, suggesting that circulation due to the shed wake dominates the unsteadiness in phase with acceleration, over added mass effects. For attached flow, the effect of unsteadiness is comparatively much smaller. At low frequencies a phase lead over the velocity is observed, compared to a lag at higher frequencies. Multiple frequency oscillations are also briefly considered. Reconstruction of the multi-frequency response using both the steady flow measurements, and the single frequency measured response, is shown to offer a relatively good fit when the flow is attached, for lower frequency combinations.

1. Introduction, critical review and aim

Unsteadiness in the onset flow is a dominant driver of both ultimate and fatigue loads of tidal turbine blades, which arises from the phenomenon such as turbulence, surface waves, and the depth-wise variations in the mean flow. Characterising these loads is crucial if tidal turbines are to meet their intended service life of at least 20 years and prove to be economically competitive with other renewable energy technologies. The vast majority of the literature has been, however, predominantly focused on characterising the steady thrust loads for tidal turbines, with the flow attached across the blades (see Bahaj et al., 2007a,b; Myers and Bahaj, 2006, 2007). Unsteady loading, particularly on the blades, where acceleration effects cannot be neglected, is inherently more complex and comparatively much more poorly understood. This is due, in most part, to the difficulties in performing experiments at sufficiently large scale to permit the underlying unsteady hydrodynamics to be accurately studied. The lack of confidence in describing the unsteady loads has unsurprisingly resulted in industrial design standards for tidal turbines currently not yet having rigorous methodologies available for analysing unsteady loading. Designers of turbine blades subsequently have limited guidance in assessing the ultimate loads and fatigue. As reported by Marsh (2009), this has led to significant levels of over-conservativeness being employed in early generation devices, which ultimately must be reduced.

The objective of this present study is to experimentally analyse the out-of-plane blade-root bending moment (defined as being about an axis normal to the rotor axis) response to harmonic axial motion, deemed representative of the free-stream velocity perturbations induced by the unsteady flow. The response to harmonic oscillatory motion is of interest for various reasons. Stochastic approaches are typically employed in fatigue calculations, and the application of an inverse Fourier analysis can lead to the computation of the impulse function itself which is very difficult to experimentally obtain, and which can be used to develop time domain based simulation models. By comparing the unsteady bending moment histories with reconstructions using the loads acquired for steady flow, as well as from theoretical predictions of oscillating airfoils, an attempt is made to quantify the relative influence of flow acceleration and subsequently the various underlying unsteady hydrodynamic load constituents. This will assist blade designers in evaluating the level of complexity required in their load prediction models, as well as providing a useful data set from which to validate and improve existing models.

The unsteady hydrodynamic blade loads arise from both circulatory and non-circulatory phenomenon. Leishman (2002) suggests that the circulatory forces are associated with the response of the induced velocity from a combination of vorticity contained in the shed wake at the blade element, and circulation in the trailed wake. The trailing wake component is considered to dominate at

* Corresponding author. Tel.: +64 9 373 7599x88146; fax: +64 9 373 7479.
E-mail addresses: imil015@aucklanduni.ac.nz (I.A. Milne), sandy.day@strath.ac.uk (A.H. Day), r.sharma@auckland.ac.nz (R.N. Sharma), r.flay@auckland.ac.nz (R.G.J. Flay).

0029-8018/$ - see front matter © 2012 Elsevier Ltd. All rights reserved.
http://dx.doi.org/10.1016/j.oceaneng.2012.12.027

low frequencies, and is associated with a dynamic inflow effect. The interaction between the shed wake and dynamic inflow effects is complex but each contribution is typically treated separately, due to dynamic inflow having a longer time scale of 1–1.5 rotor revolutions compared to 0.1 rotor revolutions for the shed wake phenomenon. The non-circulatory or true added mass forces are present due to the pressure forces which are required to accelerate the fluid in the vicinity of the blade element. This results in a force which opposes the acceleration of the flow, and therefore a positive out-of-plane bending moment. As Whelan (2010) discusses, the added mass effect is likely to be more significant for tidal turbines compared to wind turbines, as the fluid and structural densities are of the same order of magnitude. In unsteady flow the stall behaviour can also differ significantly from the steady flow cases; in that the separation and reattachment of the flow occurs at higher and lower effective angles of attack respectively, and results in large loads. Leishman (2006) discusses that dynamic stall is highly non-linear and is typically associated with both a dynamically induced camber effect, which acts to delay trailing-edge separation, and the formation and shedding of a leading edge vortex, which induces a pressure wave over the upper surface of the airfoil and subsequently leads to larger normal forces.

Experiments reported by Maganga et al. (2010) provide an insight into the general response of a tidal turbine exposed to fluctuating thrust resulting from unsteady flow. An increase in the mean thrust load on the structure of approximately 15% was observed at typical operating states, as the turbulence intensity of the flow in a flume was varied from an ambient 8% to 25%. However, the spectral characteristics of the unsteady flow and dominant length-scales were not reported, and it is therefore difficult to infer the corresponding full-scale loading. Galloway et al. (2010) have also reported on experiments on a tidal turbine, towed at constant velocity in a still-water tank and subjected to surface waves. Whilst the blade loads, again, were not specifically studied, for relatively small waves of approximately 1.6 m full-scale, the cyclic shaft thrust range was relatively large and of the order of 37% of the mean. For horizontal axis tidal turbines, which are the focus of the study here, the fluctuations in the individual blade loads can also be much more severe than the rotor thrust loads, which tend to average out the unsteady blade loads when the flow is non-coherent across the rotor.

Inferring the hydrodynamic loading on the rotor from shaft measurements, however, has the additional complication that the contributions from the shaft and hub inertia, as well as bearing friction, must be accounted for. As is the case for the experiments performed in the present study, Barltrop et al. (2006) used instrumented blades to directly measure the blade-root bending moment response. They reported on a set of experiments in a still-water towing tank, in which the forward speed of the carriage represented the mean velocity of the current, whilst the turbine was subjected to velocity perturbations resulting from surface waves. The dynamic load amplitudes were found to be 50% and 100% of the mean, in the out-of-plane and in-plane directions respectively. For relatively linear waves and attached flow, the bending moment time histories were found to compare reasonably well with a quasi-steady numerical, blade-element momentum model, with no acceleration effects included. This again suggests that unsteady influences were relatively small. Under such conditions the incident flow is therefore relatively uniform over the rotor and suited to planar oscillatory tests.

Whelan (2010) conducted an experimental investigation of the dynamic thrust response of a 300 mm diameter scale tidal turbine to harmonic axial motion, in an attempt to establish the magnitude, and relative contributions of true added mass and dynamic inflow for attached flow. The experiments were performed by surging the turbine test rig on a carriage in a flume and measuring the thrust load on the support structure. This motion, as is the case for the experiments presented in this paper, was considered to induce an oscillatory heaving motion on the blade section. It was found that the total axial inertia effects were considerably smaller than the unsteady thrust in-phase with velocity, but comparable to the solid inertia and were therefore important for control and fatigue calculations. Whilst Whelan's study showed promise, the experimental test rig was subject to a variety of complications (speed control, etc.) and the use of a rather small flume resulted in high blockage factors which could have compromised the results. As true added mass and dynamic inflow both act in-phase with the acceleration, it was not possible to separate the two effects experimentally at the frequencies considered. Comparisons were subsequently made with linear unsteady airfoil theory of Theodorsen (1935), and the returning wake extension by Loewy (1957), in which the circulatory term was considered to be associated with dynamic inflow. These suggested that, at the model scale employed, the magnitude of the contribution from the two effects were approximately equal, but the circulatory estimates tended to be less applicable to full-scale devices, for which a lag was instead predicted.

The authors are unaware of the literature directly pertaining to dynamic stall of tidal turbines. Insight into the phenomenon associated with stall is instead directed to works in the helicopter and wind turbine contexts (see Shipley et al., 1995). The majority of the experimental studies used to infer dynamic stall phenomenon involve wind tunnel tests of 2-D airfoils typically oscillating in pitch, with relatively limited literature available for heaving motion. Pitch oscillations of the NREL S814 airfoil, used in this experiment, were reported by Janiszewska et al. (1996). They have shown the maximum lift coefficient to be up to 110% higher than the steady-state value for a $\pm 10^{\circ}$ oscillation in angle of attack.

Several relevant issues are cited by researchers, following their investigations of dynamic stall. Leishman (2006) discusses that the response can differ between forcing conditions for the equivalent effective angle of attack. This is considered to be due to pitch oscillations giving rise to a lower leading edge pressure gradient compared to oscillations in heave, such that the conditions which instigate separation are experienced at higher angles of attack. Hansen et al. (2004) have commented that leading edge separation is typically not a dominant phenomenon for thick airfoils such as those used on wind turbines, which is also likely to be the case for tidal turbine foils. The effect of three-dimensionality on the stall process for a rotating wind turbine blade at a Reynolds number of 300,000 was investigated by Barnsley and Wellicome (1992). Delays in the loss of the leading edge suction peaks were observed, which resulted in enhanced lift incidence over 2D behaviour. Du and Selig (1998) have also reported on finding a slight delay in separation for a rotating blade, leading to increased lift. The events associated with dynamic stall have proved challenging to model. The frequently cited Beddoes–Leishman model (see Leishman and Beddoes, 1986, 1989; Hansen et al., 2004, specifically for wind turbines airfoils) combines Theodorsen's model for the unsteady attached flow dynamics, with empirical models for the delay in separation and movement of the vortex. If empirical models are to be employed by tidal turbine designers there is an apparent need for experimental data of dynamic stall events of tidal turbines blades for validation purposes.

1.1. Aim

Tidal turbine developers need to establish the operating conditions in which the unsteady loads become significant and dynamic stall is likely to be instigated, and subsequently the load ranges which result. The likely errors which may be incurred by using a quasi-steady

approach to predict these fully unsteady loads also need to be quantified.

In light of these issues, the objective of the present study is to develop an experiment methodology designed to examine the specific issues of uniform unsteady flow over the rotor of a tidal turbine, and to present results for out-of-plane blade root bending moments for periodic flows including dynamic stall.

2. Experimental set-up and data acquisition

2.1. Selection of experiment methodology

Several methodologies were considered prior to adopting the preferred strategy, drawing on the issues cited in previous studies in the literature. Compared to a two-dimensional wind-tunnel test of a heaving foil, the flow around a rotating blade, of finite span, is likely to exhibit additional three dimensional effects which may be expected to result in differences from the stall characteristics of a 2-D infinite foil. It is acknowledged that the effects are more pronounced at inboard sections, which have a relatively low contribution to the rotor load. Hence it may be argued that while such tests provide valuable data, the flows are too highly simplified to allow direct application in the context of tidal turbines.

Furthermore, testing turbines in surface waves involves a highly complex flow varying over the rotor plane, which may be compromised by free surface effects, and limited by achievable wave height. In order to achieve an appropriate and controllable unsteady flow which is uniform over the rotor plane, it seems most beneficial to oscillate the turbine axially in the flow. However, if this is combined with a mean velocity generated by the current in a flume, boundary layer effects and background turbulence can lead to non-uniformities in the flow, unless the flume is extremely large and well-conditioned. Whilst there is no Froude–Krylov force component in cases where the rotor is oscillated in still water, the relatively low thickness of a blade section would imply that the effect is negligible.

The most promising approach for generating an unsteady flow with the appropriate level of complexity appears to be by super-imposing an unsteady surging motion upon a steady forward speed in calm water in a towing tank. This approach is adopted in the present study. Inducing a coherent loading over the rotor plane is, perhaps, an idealisation of the flow in nature, apart from that due to relatively long waves or large scale eddies. However, it is an attempt to reduce an already complex situation, whilst providing useful data from which to study the underlying hydro-dynamics as well as to validate models. Assessing the blade loads, as opposed to the hub loads, is also considered to be more relevant. Connell (1982) has shown that rotational sampling of turbulence can induce a coherent load over a substantial region of the blade span, at frequencies corresponding to multiples of the rotational frequency.

2.2. Specifications of the towing tank and carriages

The experiments for this present study were conducted at the University of Strathclyde's Kelvin Hydrodynamics Laboratory towing tank (76 m × 4.6 m × 2.5 m). For all tests the water depth was maintained at 2.23 m. The effect of reflective waves is mitigated using a 9 m long beach installed at one end of the tank, with reflection coefficient typically less than 5%. The main carriage velocity is computer controlled, and was ramped up at constant acceleration at the start of each test, and then maintained constant for the duration of the test period, before being ramped down again.

The main carriage is equipped with a digitally controlled auxiliary carriage. The auxiliary-carriage is driven by a linear actuator, and with a comparatively low inertia compared to the main carriage, accelerations in the order of up 2g can be realised. Velocity is limited to 2 m/s, whilst displacement has a range of 1.0 m. For the present tests a simple harmonic displacement time history of frequency f was input into the computer controlling the sub-carriage, such that the desired velocity upstream of the turbine $u(t)$ was of the form

$$u(t) = U + \tilde{u}\,\sin(2\pi ft), \tag{1}$$

where U is the velocity of the main carriage (assumed constant), and $\tilde{u}$ is the maximum velocity of the auxiliary carriage. A schematic of the test set-up is shown in Fig. 1, and the turbine as installed on the two carriages can be observed in Fig. 2.

2.3. Specifications of the rotor and blades

A horizontal-axis, tri-bladed rotor was used in the experiments, which had a rotor and hub diameter of 780 mm and 120 mm respectively, and is shown in Fig. 3. The blockage of the rotor based on the projected frontal area was relatively low at 4.7%, compared to the previous studies such as Bahaj et al. (2007a). In light of this, no correction to the experimental data was deemed to be necessary.

The blades have a non-uniform profile, with the chord and twist varying along the span, as depicted in Fig. 4. The blade sections conform to the 24% thick, NREL S814 profile, which as discussed by Janiszewska et al. (1996), are favoured for their relative insensitivity to surface roughness and ability to generate relatively large lift, whilst providing the necessary structural stiffness. The three blades were instrumented with water-tight strain gauges on the

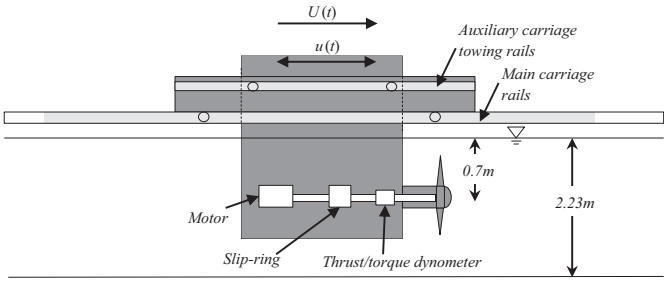

Fig. 1. Schematic of the turbine and experimental test configuration.

Fig. 2. Photo of the turbine as installed, with the main and auxiliary carriages visible.

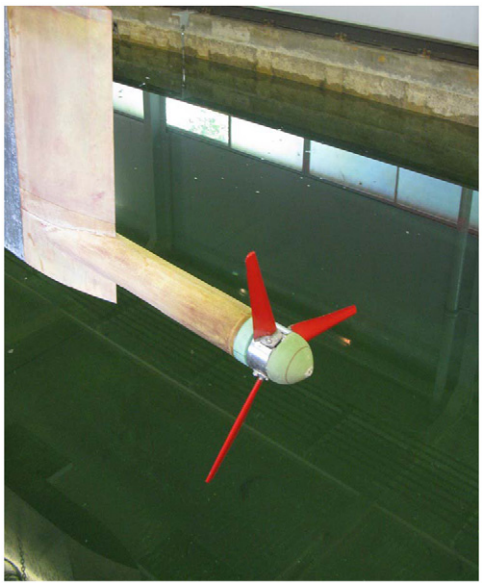

Fig. 3. Photo showing the rotor and blades prior to installation on the carriage.

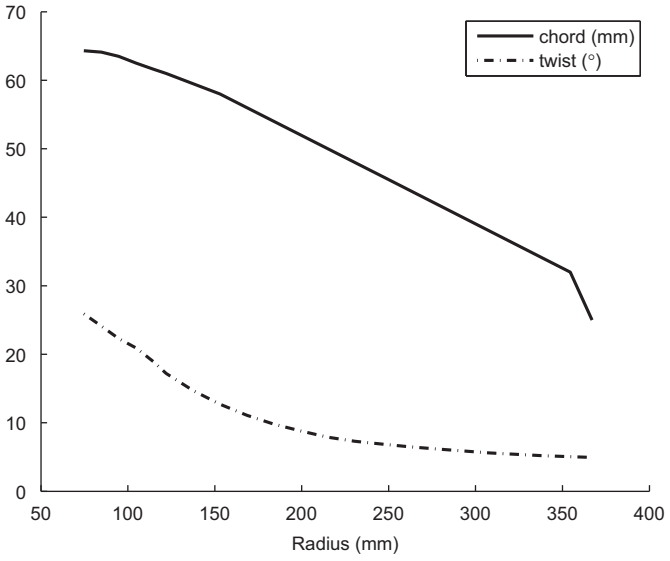

Fig. 4. Chord and twist profile of the blade.

cylindrical blade root, at a radius of $r_{sg}=36$ mm from the rotor axis, and which were enclosed within the rotor hub. The out-of-plane bending moment from one of these blades is analysed in this study.

The rotor motor, slip ring, and thrust and torque transducers were enclosed in a submerged rectangular box, at a distance of approximately 2 diameters downstream of the rotor. The box was mounted rigidly to the sub-carriage from above, and the rotor axis was 0.70 m below the mean free water surface.

A number of strategies were considered for the speed control of the rotor. A closed-loop constant torque system would require the measured shaft torque to be incorporated in the control system, and this was deemed to be potentially problematic in the context of an already complex system. Using a generator to control speed effectively restricts the experiment to the simulation of behaviour of a particular system, which is in conflict with the aim of generally applicable idealised hydrodynamics. Hence, tests were performed at constant rotational speed, using a closed-loop digital controller. The oscillatory motion of the sub-carriage therefore induced a perturbation in both the tip-speed ratio $\lambda(=\Omega R/u)$, where Ω is the rotor speed, R is the blade-tip radius, and the rotor torque Q.

2.4. Data acquisition, filtering and repeatability

A Cambridge Electronic Design Power1401 data acquisition system, with a sampling rate of 400 Hz was used to acquire all signals, except the velocity of the main carriage. A low pass digital filter with a cut-off frequency of 300 Hz was applied in real time on all signals. For each oscillatory test, the auxiliary carriage motion commenced whilst the main carriage was accelerating. This facilitated the decay of transients in the sub-carriage and blade loads sample histories, therefore allowing for longer test runs.

Spectral analyses of the carriage velocity and acceleration showed that whilst structural vibrations were minimal, energy peaks at multiples of the dominant frequency were also present, notably at $5f$ and $7f$, as is demonstrated in Fig. 5. This was a result of irregularities in the carriage response, deemed to be caused by physical limitations with the actuator, and tended to become more severe with increased frequency and a decrease in oscillatory amplitude. As is also shown in Fig. 5 these spikes were also present in the spectra of the bending moment. However, in the case where flow separation occurs, the energy at $2f$ is more significant than that due to the carriage irregularities.

An IFR 5th order Butterworth digital filter was applied off-line to all signals co-currently, and in both forward and backward directions to eliminate any phase error. The effect of cut-off frequency is shown in Fig. 6, and a cut-off of 4 times the highest oscillatory frequency was ultimately applied to all signals, which was found to reduce the majority of erroneous noise, whilst ensuring that the stall events and dominant non-sinusoidal motions were retained. Inherent in applying such a filter is the assumption that the higher frequency components do not contribute significantly to the underlying stall phenomenon, such as the location point of separation and reattachment.

As can also be inferred from Fig. 6, the oscillations were found to be highly repeatable. Over the duration of each test minor differences were, however, typically observed in the individual load cycles, notably when stall was present. There appears to be

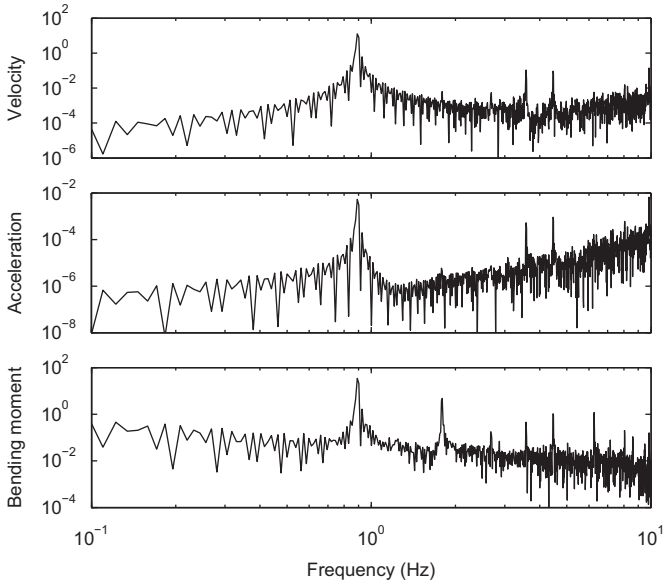

Fig. 5. Example of single-sided normalised auto-spectral densities ($fS(f)/\sigma^2$) of the velocity, acceleration and the bending moment. Increased energy is evident at multiples of the oscillation frequency.

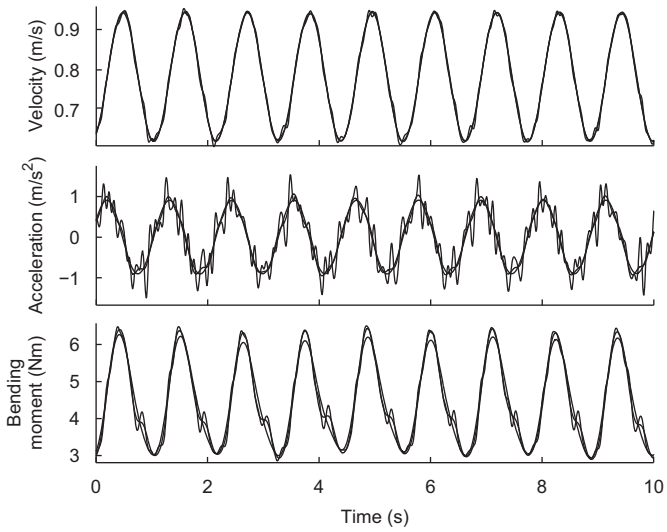

Fig. 6. Effect of the filter cut-off frequency on the oscillatory velocity, acceleration and the bending moment time history, for $f_c = 2,4,10f$. Flow separation and stall can be observed.

no obvious correlation between these load irregularities and the velocity, rotational speed, or to the relative position of the blade in the water column. It is believed that the differences could arise from either the experimental set-up, such as background unsteadiness in the towing tank induced by the oscillating carriage, or alternatively it may be due to the unsteady flow phenomenon. For instance, recalling that dynamic inflow typically has a time scale longer than one oscillation, this effect may be periodically disrupted by flow separation.

3. Uncertainty analysis

An uncertainty analysis has been attempted to estimate the dominant experimental errors in the measurement of blade root out-of-plane bending moment, its non-dimensional coefficient C_{M_y}, defined in Eq. (2), and the tip-speed ratio λ.

$$C_{M_y} = \frac{M_y}{\frac{1}{2}\rho A U^2 R}, \tag{2}$$

where ρ is the density of water and A is the frontal area of the rotor.

The authors are unaware of existing literature on the uncertainties analysis specific for unsteady tidal turbine tests. In lieu of this, the methodology used is based on that presented by Coleman and Steele (2009) and ITTC (2008a,c). The uncertainties of a variable X are categorised as being either systematic (b_X), in that they are inherent in all tests, or random (s_X), and varying between each test. The total uncertainty of variable X is given as

$$u_X^2 = s_X^2 + \sum_{k=1}^{M} b_k^2, \tag{3}$$

where k is the number of systematic sources of uncertainty.

The sources of systematic errors implicit in the measurements of the root out-of-plane bending moment are considered to be composed of three dominant uncorrelated elemental errors. These are due to calibration of the strain gauge using M1 standard weights ($b_{My,calib} = 0.015$ N m) and a lever arm, scatter in the least-square fit of the strain gauge calibration ($b_{My,curvefit} = 2SEE = 0.008$ N m), and the 16-bit analogue-digital conversion of the signal ($b_{AD} =$ 0.00006 N m). The total systematic error was estimated using the Taylor series method for propagation to be $b_{My} = 0.017$ N m, with the calibration uncertainty, and more specifically the uncertainty from the weights, contributing to nearly 100% of the error. Transient effects from the sensors are considered to be small as the strain gauges have a first order response.

The main carriage speed was measured using both an encoder on the driving motor and via a counter on the trailing wheel of the carriage. The sub-carriage velocity was computed by applying the central difference method to the actuator displacement. Ascertaining the systematic uncertainties associated with both the main carriage speed and sub-carriage velocity is challenging due to the complexities inherent in the systems, and physical difficulties involved in measuring the key components. Direct comparisons between the two measurement sources tend to agree well. As a case in point, for a desired speed of $U = 0.894$ m/s, which is the maximum mean speed used in the oscillatory tests, the measurements from the encoder and trailing wheel from one particular run were 0.13% greater and 0.4% lower respectively. The encoder measurement was however, generally deemed to be more accurate and used in all tests. Furthermore, previous experiments have shown that the speed measurements are within the thresholds recommended by ITTC (2008b) for resistance tests, and the authors therefore conservatively assume that the systematic uncertainties for both carriages are $b_U = b_u = 3$ mm/s.

The rotor blades were manufactured from aluminium alloy using a CNC machine, with a tolerance of $b_R = 0.5$ mm. The temperature was measured with a probe to an accuracy of 0.1 °C. Following ITTC (2006) at a typical tank temperature of 16.0 °C, the uncertainty in the fresh water density is estimated as $b_\rho = 0.021$ kg/m^3. The systematic uncertainty of the bending moment coefficient was also predicted using the Taylor series method for propagation. For a typical test case at $U =$ 0.894 m/s, where the bending moment is $M_y =$ 6.60 Nm, it is estimated to be $b_{C_{My}} = 0.0006$. The uncertainty associated with the blade radius being approximately twice the magnitude of the velocity and bending moment, with negligible contribution from the uncertainty in density. In terms of the tip-speed ratio, the rotational speed of the rotor was calibrated by comparing the output measured by the tachometer with a pulse count obtained by a proximity sensor attached to the shaft, in which the uncertainty was predicted as $b_\Omega = 0.036$ rpm. The systematic uncertainty for the aforementioned speed is hence estimated as $b_\lambda = 0.012$, with the uncertainty associated with velocity contributing to nearly 100% of the error.

The random uncertainties, for a 95% confidence level, were estimated from multiple repeats of three test cases, a steady carriage test for $U = 0.89$ m/s, $\lambda = 3.6$; and two oscillatory tests, for $U = 0.78$ m/s, $\lambda = 3.6$, $f = 0.9$ Hz, $\mu = 0.2$, and $U = 0.89$ m/s, $\lambda = 3.6$, $f = 0.45$ Hz, $\mu = 0.2$. A summary of the estimates of these uncertainties, and their source are listed in Table 1. For the two oscillatory cases, the uncertainty associated with the bending moment and auxiliary carriage velocity has been computed from the root-mean-square of the response, as opposed to the mean value used for all the other parameters. Between four and five repeat runs were conducted for the cases, all near the end of the entire test program. A relatively small (approximately 2%), but notable difference was observed in mean and, for the unsteady tests, also in the minimum values of the out-of-plane bending moment between repeats performed at the initial and final stages of the test program. Similar differences were also found for the shaft thrust, torque and in-plane bending moment measurements. It is therefore believed that this difference is primarily due to a systematic error in the bending moment measurement, and likely a result of an unbeknown small pitch angle change during the removal and re-installation of the turbine rig on the carriage, which was conducted once, prior to performing the repeated runs. Subsequently, the random uncertainty of the bending moment and its coefficient for the initial run were not included in the estimates.

In general, the uncertainties are considered to be sufficiently small for the purposes of the analyses presented herein in this study.

4. Steady velocity experiments

As an initial step in quantifying the role of unsteadiness, in providing a base-line from which to reconstruct a quasi-steady based response with no acceleration component, the performance of the rotor and loads have been characterised for steady carriage velocities. The tests were performed at constant rotor speeds between 67 rpm and 96 rpm and carriage speeds between $U=$ 0.45 and 1.01 m/s. Using Froude number based scaling, in which $U_{FS}=U\sqrt{h_{FS}/h}$, where h is the water depth, and it is assumed $h_{FS}/h=20$, these speeds are equivalent to $U_{FS}=2$–4.5 m/s full-scale. Issues with water spillage from the tank imposed an upper limit on the carriage velocity and hence the minimum tip-speed ratio able to be considered. The time averaged power $P(=\Omega Q)$, thrust T, out-of-plane (M_y) and in-plane (M_x) blade root bending moment coefficients, as a function of tip-speed ratio are shown in Fig. 7, with C_P and C_T defined as

$$C_P=\frac{P}{\frac{1}{2}\rho AU^3}, \tag{4}$$

Table 1
Sources of random uncertainties and their magnitudes associated with the measurement of the out-of-plane root bending moment and its coefficient.

Source	Steady	Oscil 1	Oscil 2
Bending moment ($\times10^{-4}$ N m)	6.5	1.8	1.6
Main carriage velocity ($\times10^{-5}$ m/s)	39	2.8	60
Oscillatory velocity ($\times10^{-5}$ m/s)	–	1.9	0.98
Rotor speed ($\times10^{-3}$ rpm)	5.0	5.0	57
Bending moment coefficient ($\times10^{-5}$)	2.5	0.4	3.4
Tip-speed ratio ($\times10^{-3}$)	1.6	0.3	3.1

$$C_T=\frac{T}{\frac{1}{2}\rho AU^2}. \tag{5}$$

The performance of the rotor is characterised by a relatively steep decay in the coefficients at low tip-speed ratio, where stall effects are dominant, whilst at higher-tip speed ratios the coefficients are influenced by drag forces, and the rotor nears the turbulent wake state. As is discussed by Leishman (2006), this turbulent wake state is characterised by an enhancement in wake turbulence and aperiodicity, and the onset flow perceives the rotor as an increasingly solid disc. This leads to a reduction in the power coefficient, but an increase in the thrust and out-of-plane bending moment coefficients. The optimal power coefficient is attained at a tip-speed ratio between approximately $\lambda=3$ and 4. The magnitude of the out-of-plane bending moment coefficient is considerably larger than the in-plane component, and as has been previously cited in the literature (see Fraenkel, 2007), is indicative of the dominance of the thrust forces over the gravitational and centrifugal inertia forces. The out-of-plane loads are hence only considered hereafter in the unsteady analysis presented in this paper.

The coefficients also exhibit sensitivity to the rotational speed. The mean Reynolds number for a blade section at $0.75R$ is predicted to vary from approximately 100,000 to 70,000 between rotor speeds of 96 rpm and 63 rpm. In lieu of airfoil data for these Reynolds numbers, it is postulated that the lift and drag performance of the foil would have reduced as the rotor speed is slowed, and the boundary layer nears a laminar flow regime. Laminar separation bubbles are also expected to be present on the airfoil surface, which will result in increased drag. An experimental wind tunnel based study is currently being conducted to verify this. The increase in the thrust and out-of-plane bending moment coefficients at high tip-speed ratios (i.e. $\lambda\gg5$) for the low rotor speed cases may be due to the influence of the turbulent wake state, where the thrust forces are more sensitive to global drag effects, rather than to the flow over the blade section.

The ratio of the rotor thrust to the out-of-plane bending moment ($3M_y/TR$) has also been computed, and is shown in

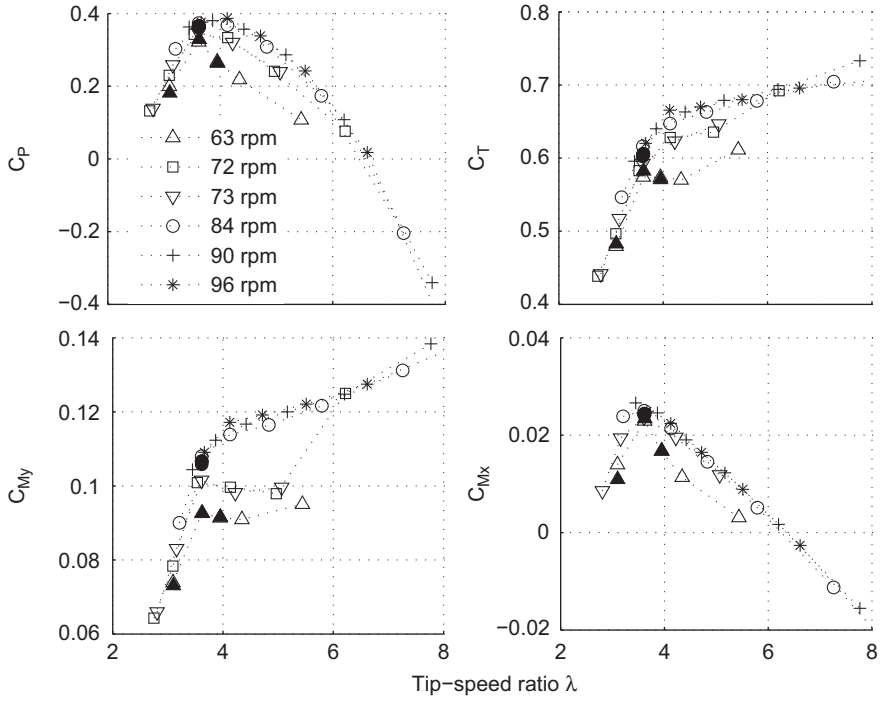

Fig. 7. From top: coefficients of rotor power, thrust, blade root out-of-plane and in-plane bending moments, all for steady carriage motion. Solid symbols donate repeats.

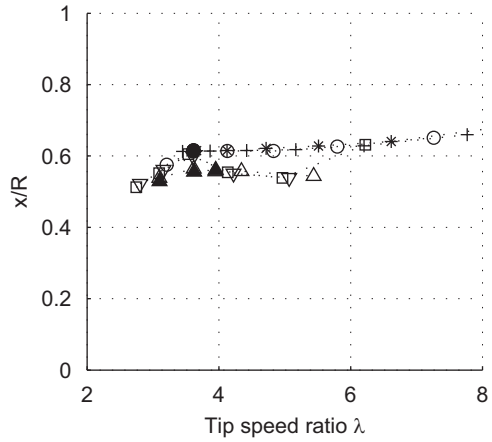

Fig. 8. The effective radius of the applied out-of-plane bending moment normalised by the blade span ($3M_y/TR$), for steady carriage motion. Solid symbols donate repeats.

Fig. 8, which provides means of ascertaining the effective centre of loading. The ratio is approximately 0.62, which agrees qualitatively with that predicted for an ideal rotor, presented by Hansen (2008). Inherent in the approach, however, is the assumption that errors due to the blade root strain gauge not being located at the rotor axis are small, and which will result in an ratio estimate that is likely to be of slightly smaller magnitude.

5. Oscillatory experiments

5.1. Parameter selection

In an effort to ensure that the results of this study are applicable to the tidal turbine industry, the axial velocity oscillations which were tested are representative of those likely to be imposed on a tidal turbine operating in the presence of surface waves and large scale turbulence. Whelan (2010) has indicated that large waves with periods of 9 s may induce velocity fluctuations of up to 2 m/s. Milne et al. (in press) have shown that the turbulence intensity at a typical tidal turbine site is of the order of 10–15%, with dominant time scales of 6–10 s.

Applying Froude based scaling, the frequencies of interest here range from $f=$ 0.45 Hz to 1.56 Hz, whilst the oscillatory amplitudes are typically between 0.1 and 0.2 times the mean flow speed. Whelan has also previously highlighted the various scaling parameters applicable to unsteady load testing for tidal turbines. The Current number $\mu(=\tilde{u}/U)$, defined as the ratio of the maximum oscillatory velocity to the mean upstream velocity, and akin to the turbulence intensity, provides a means of scaling the oscillatory velocity amplitudes. The expected range of full-scale Current numbers of 0.1–0.3 are able to be achieved in the present tests. Unsteady blade section hydrodynamics is typically characterised by the reduced frequency $k(=\pi fc/\Omega r)$, with values ranging from 0.01 to 0.07 likely to be experienced by a full-scale turbine at $0.75R$. Reduced frequencies in excess of $k=0.05$ are typically considered as those where unsteady forces become significant on a 2-D blade section (Leishman, 2006). For rotating blades, or returning wakes, the ratio of the oscillatory frequency to that of the rotational frequency m is useful for ascertaining the relative wake length. In contrast to Whelan's tests it was possible to obtain higher m values such as expected at full-scale.

The sensitivity to both the oscillation frequency and maximum oscillation velocity is analysed at two mean-tip speed ratios, of $\lambda=3.6$ and $\lambda=4.1$. Referring to Fig. 7, these operating points lie either side of the point of maximum power in steady flow, and are therefore deemed to be of most interest for tidal turbine designers. The investigations were conducted by varying one parameter at a time whilst maintaining the others nominally constant, to aid the inference of the underlying hydrodynamic phenomenon.

5.2. Sensitivity to forcing conditions

The response for a mean tip-speed ratio of $\lambda=3.6$ is first considered, for which the response is affected by pronounced flow separation. Shown in Figs. 9 and 10 are the velocity, acceleration and bending moment coefficient time histories for a variation in oscillatory frequency from $f=$ 0.50 to 0.89 Hz, and a variation in Current number between $\mu=0.1$ and 0.3. These are cycle median-averaged histories and plotted as a function of non-dimensional time $\tau(=t/T)$. For these cases the mean flow velocity was fixed at two flow speeds of $U=0.78$ m/s and $U=0.89$ m/s, where the mean rotor speed was 73 rpm and 84 rpm respectively. As can be observed, the oscillatory motion able to be produced is relatively good, given the complexity of the system. However, the $U=0.78$ m/s cases tend to exhibit greater irregularity in the oscillatory motion, notably for a current number $\mu=0.1$. This is likely to be due to the aforementioned physical limitations of the actuator, and provides a lower limit on the oscillatory parameters that can be studied. However, these cases still provide a useful insight into assessing the effect of unsteadiness.

The bending moment responses exhibit phenomena associated with separated flow and dynamic stall, with key stages involved in the process highlighted as 1–3. Following Leishman (2006), at stage 1, the bending moment exceeds the point of stall observed for steady flow conditions, and there is a delay in the onset of flow separation due to induced camber, the influence of the shed wake and the unsteady boundary layer response. Stage 2 indicates the point of full separation, which occurs after the flow separation point has shifted from the trailing edge to the leading edge. An increase in oscillatory frequency delays the movement of the separation point, and subsequently the point in the cycle at which full separation occurs. The magnitude of the bending moment can be observed to be significantly greater than that for steady stall, as also shown in Figs. 9 and 10, and being approximately 25% greater for the highest frequency cases for $U=0.78$ m/s. An increase in frequency can also be observed to delay the onset of flow reattachment, which is indicated as stage 3. For the highest frequency cases, the reattachment occurs near the point of minimum velocity, suggesting the flow separation can be present for a significant portion of the load cycle. An increase in the current number also results in a delay in stall to lower tip-speed ratios, as well as the reattachment to higher tip-speed ratios. When the flow is attached, the agreement with quasi-steady predictions is relatively good, highlighting that the unsteady contribution in attached flow is much smaller compared to that due to separated flow.

The contribution from the forces out of phase with velocity alone can be inferred qualitatively by plotting the bending moment as a function of tip-speed ratio, in the form of hysteresis loops, since the rotor is operating at constant speed. The hysteresis loops in Fig. 11, for the aforementioned cases, clearly demonstrate the complex time dependent nature of flow separation, with significant variations in the instantaneous phase. The phase of the hysteresis loops in attached flow can also be observed to be frequency dependent. For the two lowest frequency cases at $U=0.89$ m/s the dynamic bending moment is observed to lead the velocity during the complete oscillation cycle. As the frequency is increased, the phase, and therefore the relative magnitude of the load in-phase with acceleration, reduces, and for the highest frequency case a lag can be observed when the flow is attached. For the $U=0.78$ m/s cases a lag is

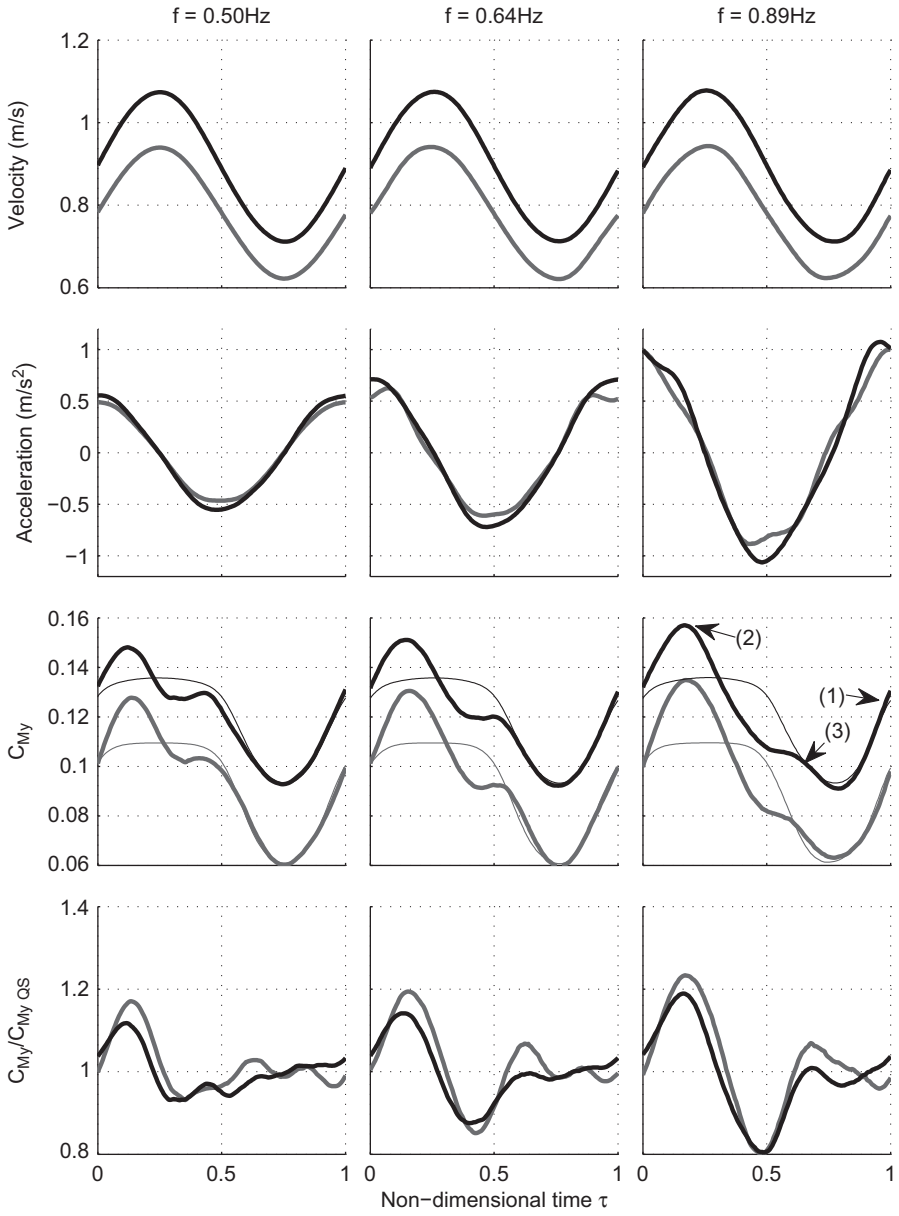

Fig. 9. Time histories of the velocity; acceleration; out-of-plane bending moment coefficient, with a quasi-steady reconstruction based on the loads for steady flow superimposed (thin lines); and ratio of the bending moment to the quasi-steady reconstruction; demonstrating the effect of oscillatory frequency for a nominal Current number $\mu = 0.2$. Oscillations performed at a mean tip-speed ratio of $\lambda = 3.6$ and flow speeds of U=0.78 m/s (grey) and U=0.89 m/s. The bending moment coefficient is offset by 0.02 for the U=0.89 m/s case for clarity.

observed for attached flow at all the frequencies analysed. It is postulated that this lag signifies a dominance of shed wake circulation over unsteadiness due to true added mass and the trailed wake associated with dynamic inflow, both of which imply a lead over the velocity.

The oscillatory tests conducted at a mean tip-speed ratio of $\lambda = 4.1$ allow for a further exploration of the unsteady loads in attached flow, and where complete flow separation is not present, or is at most very minor. The hysteresis loops for the effect of frequency and current number for mean flow speeds of U= 0.78 m/s and U= 0.89 m/s, where the rotor speed was 84 rpm and 96 rpm respectively, can be observed in Fig. 13. For the f=0.50 Hz and f=0.64 Hz cases, a phase lead is observed in the bending moment, suggesting that added mass and dynamic inflow effects dominate over the shed wake effects. The estimate of the added mass contribution is, however, indicated to be smaller than that due to dynamic inflow. A linear fit to the bending moment for the two f=0.50 Hz cases suggests that the phase lead of the bending moment over velocity is small, at approximately 1°.

However, the phase appears to be frequency dependent, as for the f=0.89 Hz case the lead is very small at high instantaneous tip speed ratios. The phase is also non-linear, suggesting that linear fits are unlikely to be very useful unless the frequency is low. Referring to the quasi-steady reconstruction, for $\mu = 0.2$ cases, as the instantaneous tip-speed ratio is reduced, there appears to be an increase in the bending moment over the load for steady flow which is synonymous with delays in the onset of separation. It is therefore postulated that this delay results in increased shed wake circulation, and ultimately a reduction in the phase during the cycle. As the rotor operation is likely to be nearing the turbulent wake state at high tip-speed ratios, there however, may also be enhanced back-flow which could lead to a reduction in the loading as the carriage is reversed. Such a phenomenon does

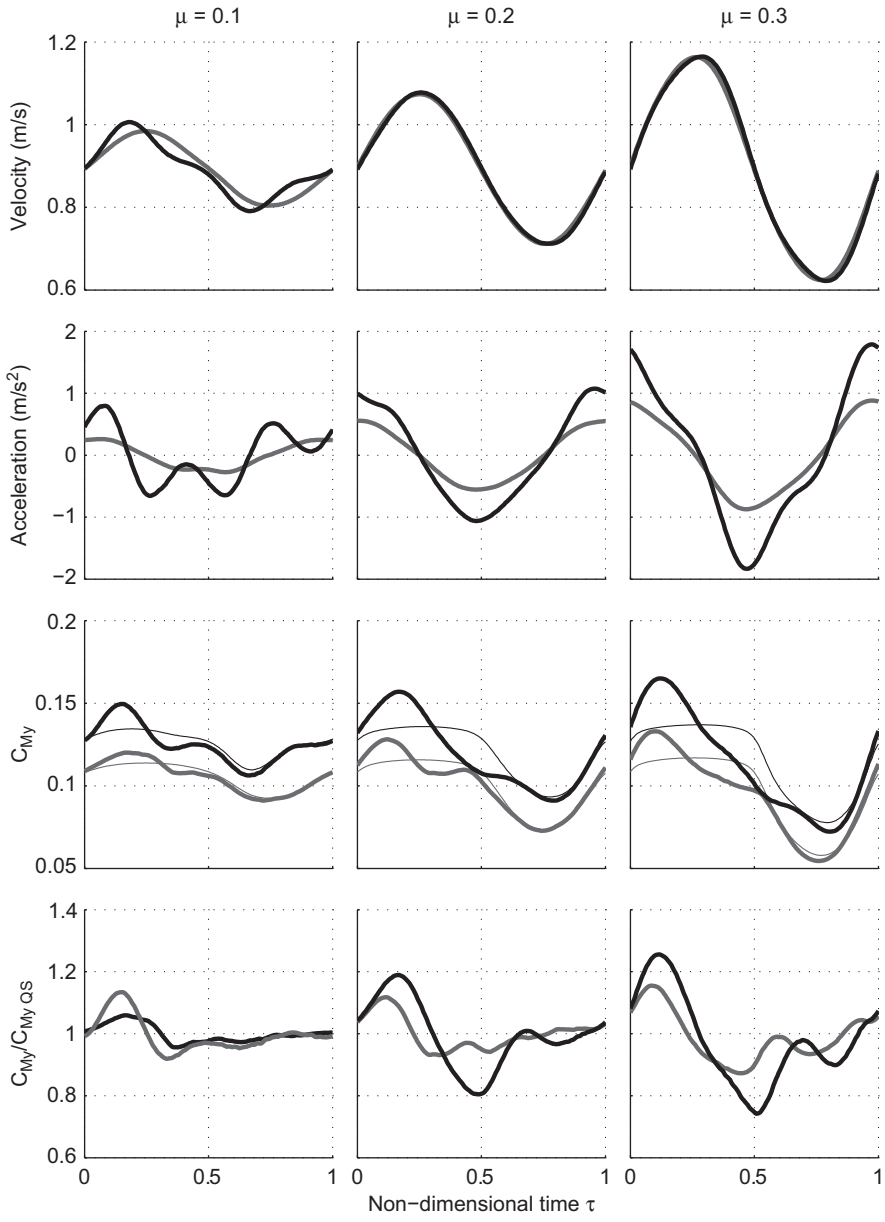

Fig. 10. Time histories of the velocity; acceleration; bending moment coefficient, with a quasi-steady reconstruction based on the loads for steady flow superimposed (thin lines); and the ratio of the bending moment to the quasi-steady reconstruction; demonstrating the effect of current number for oscillation frequencies of $f=0.50$ Hz (grey) and $f=0.89$ Hz. Oscillations performed at a mean tip-speed ratio $\lambda=3.6$ and flow speed $U=0.89$ m/s. The bending moment coefficient is offset by 0.02 for the $f=0.89$ Hz case for clarity.

not appear to be present for the low frequency oscillation, even at a current number of $\mu=0.3$ and for which 'weak' stall is present. This implies that for the parameters tested, the phase is likely more sensitive to the oscillatory frequency than the Current number.

5.3. Comparisons with unsteady foil theory

The contribution of the shed wake on the circulatory forces in phase with acceleration can be estimated for a 2-D thin foil oscillating in heave using the linear Theodorsen's theory. An attempt has been made here to compare the analytical predictions for the $\lambda=3.6$ cases at a mean flow speed of $U=0.78$ m/s and $\mu=0.2$, all for which a lag was observed when the flow was attached. Theodorsen's model has been applied on a sectional basis, with the root bending moment estimated from

$$M_y=\frac{1}{2}\pi\rho V^2\int_{r=r_{hub}}^{r=R}c(r-r_{sg})\left[\frac{c}{2V^2}\{i\omega\tilde{u}\}+2\left(\frac{1}{V}\{\tilde{u}\}+\alpha\right)C(k)\right], \quad (6)$$

where the oscillatory velocity is of the form $u=\tilde{u}e^{i\omega t}$, V is the relative velocity incident on the blade section, assumed to be equal to $V=\Omega r$, and $C(k)$ is the Theodorsen lift deficiency complex number defined as

$$C(k)=\frac{H_1^{(2)}(k)}{H_1^{(2)}(k)+iH_0^{(2)}(k)}, \quad (7)$$

where $H_\nu^{(2)}=J_\nu-iY_\nu$ is the Hankel function.

The first term in the square brackets in Eq. (6) is the non-circulatory component, or load due to true added mass, which results in a bending moment contribution that is in phase with positive acceleration. The second is that which is associated with

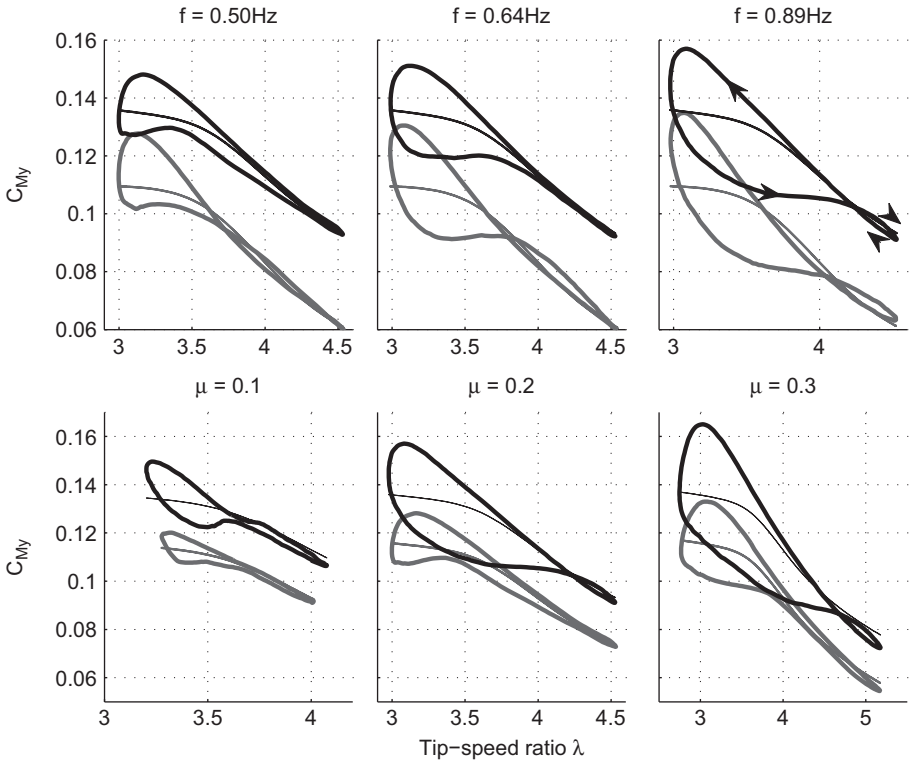

Fig. 11. Bending moment coefficient as a function of instantaneous tip-speed ratio, for a mean tip-speed ratio of $\lambda = 3.6$. Above: effect of oscillatory frequency for a Current number of $\mu = 0.2$ and flow speeds of $U = 0.78$ m/s (grey) and $U = 0.89$ m/s (offset by 0.02 for clarity); below: effect of current number, for a flow speed of $U = 0.89$ m/s and oscillatory frequencies of $f = 0.50$ Hz (grey) and 0.89 Hz (offset by 0.02 for clarity). A quasi-steady reconstruction based on the steady flow measurements is superimposed.

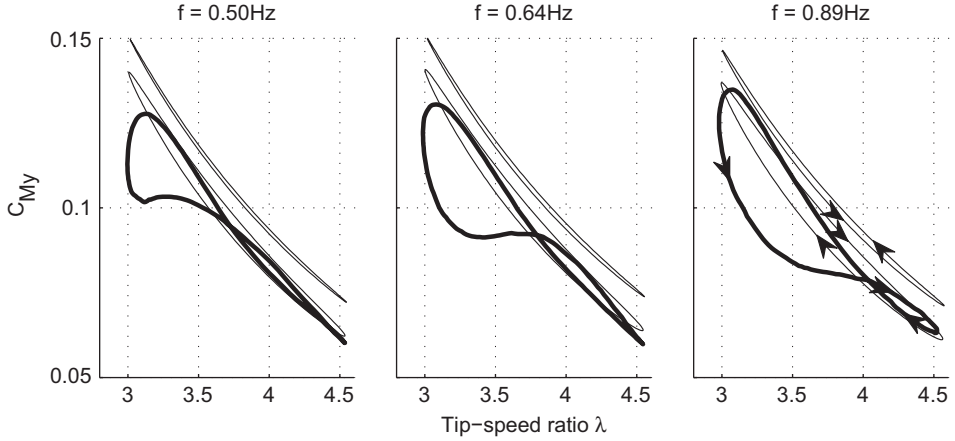

Fig. 12. Bending moment coefficient as a function of instantaneous tip-speed ratio, for a mean tip-speed ratio of $\lambda = 3.6$, flow speed of $U = 0.78$ m/s and current number $\mu = 0.2$, demonstrating the effect of oscillatory frequency. A reconstruction based on Theodorsen's theory and of the non-circulatory component (offset by 0.01) are superimposed.

blade circulation. The imaginary part of which is that due to the shed wake and acts 180° out of phase with acceleration, whilst the real term is the unsteady load in phase with velocity. The term involving the angle of attack, α is a quasi-steady contribution, and which the loads will tend towards as the reduced frequency is reduced. As α is an unknown parameter, a best-fit to the measured loops was computed and applied.

Referring to Fig. 12, it can be observed that the attached part of the cycle can be predicted reasonably well using Theodorsen's model. Also shown is the predicted contribution due to true added mass, which acts in the opposite sense to the shed wake component, and is significantly smaller. This suggests that the unsteadiness observed in the load following stall is predominantly due to the shed wake circulation, rather than true added mass or dynamic inflow. However, it must be appreciated that Theodorsen's model neglects the effect of helicity of the wake. Employing the model by Loewy (1957), which as previously stated incorporates a 'cascading' wake, though still not helical, would appear to predict a more pronounced lag and therefore may be less reliable. Three dimensional effects are also not considered, though it is postulated that their contributions are relatively small.

5.4. Multi-frequency oscillatory motion

As previously discussed, describing the out-of-plane bending moment response to single frequency oscillations is an important

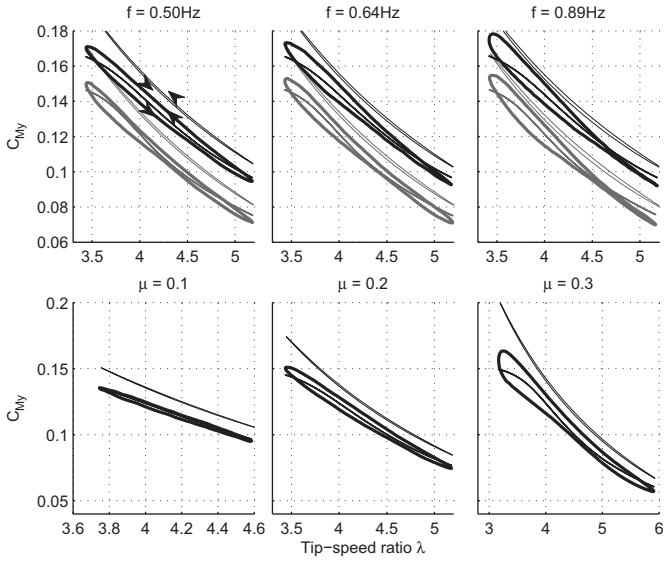

Fig. 13. Bending moment coefficient as a function of instantaneous tip-speed ratio, for a mean tip-speed ratio of $\lambda = 4.1$. Above: effect of oscillatory frequency for a Current number $\mu = 0.2$ and flow speeds of $U = 0.78$ m/s (grey) and $U = 0.89$ m/s (offset by 0.02 for clarity); below: effect of current number, for a flow speed of $U = 0.89$ m/s and oscillatory frequency of $f = 0.50$ Hz. Superimposed are quasi-steady reconstructions based on the steady flow measurements, and the non-circulatory component estimated from Theodorsen's theory (offset by 0.01 for clarity).

step towards characterising the response to more complex flows. Whilst the blade load response to single frequency oscillatory motion was the focus of the present study, a limited set of multi-frequency oscillations were performed. These tests were for a carriage velocity $U = 0.89$ m/s and tip-speed ratio $\lambda = 3.6$. Two cases are considered here, where an oscillation frequency of $f = 0.89$ Hz was combined with a lower frequency of $f = 0.5$ Hz, and a second where it was combined with a higher frequency of $f = 1.4$ Hz. The time histories of the bending moment for these cases are shown in Fig. 14, together with a reconstruction using the steady flow measurements.

For both cases, overshoots in the maximum bending moment can be observed which are indicative of flow separation. As was observed for the aforementioned single frequency oscillations, these overshoots are greater in magnitude for the higher frequency cases. The increasing dynamic bending moment can also be observed to lag the quasi-steady response as the flow begins to separate. For the higher frequency case this lag is also present for the majority of the cycle, whilst for the lower frequency combination it appears that the dynamic load begins to lead, though only slightly, once the flow is attached.

An initial attempt is made to assess the applicability of superposition, an example of which is shown here in Fig. 15, for the two aforementioned cases. For the lower frequency combination, a relatively good reconstruction has been obtained, which is due to the presence of only relatively limited flow separation. This is in contrast to the poorer fit for the higher frequency combination, in which a greater degree of separation is experienced.

6. Discussion

The results of this study aim to provide designers of tidal turbines with valuable insight into the level of complexity required in predicting the unsteady hydrodynamic blade loads. For attached flow conditions, the unsteady component is considered to be small relative to the load for steady flow. The approach proposed by draft industrial guidelines (Rules for Classification and Construction, IV Industrial Services, Part 14 – Offshore Wind Energy, Guideline for

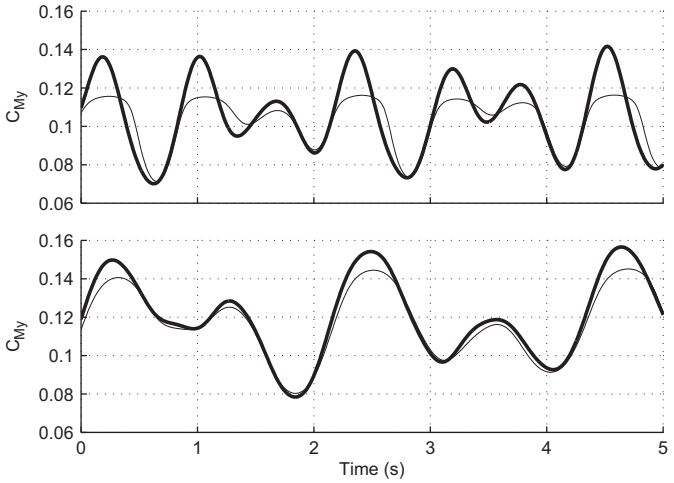

Fig. 14. Example of a multi-frequency oscillation (bold) and its quasi-steady reconstruction using the bending moment for steady flow. Mean flow speed $U = 0.89$ m/s and current number $\mu = 0.2$. Top: oscillatory frequencies $f = 0.64$ Hz and 0.89 Hz, below: $f = 0.50$ Hz and 0.64 Hz.

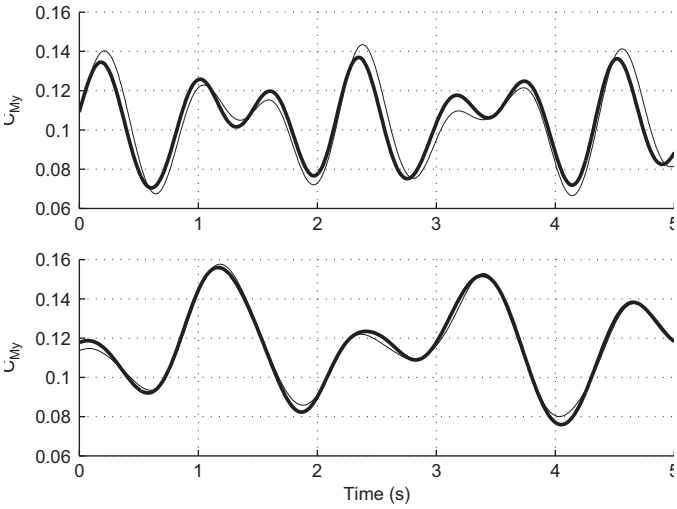

Fig. 15. Example of a multi-frequency oscillation (bold) and its reconstruction using single frequency oscillation histories. Mean flow speed $U = 0.89$ m/s and current number $\mu = 0.2$. Top: oscillatory frequencies $f = 0.64$ Hz and 0.89 Hz, below: $f = 0.50$ Hz and 0.64 Hz.

the Certification of Ocean Energy Converters Part 1 Ocean Current Turbines, 2005), accounting for the unsteady loads via a multiplication factor, is therefore likely to be reasonable. The loads are also likely to be able to be approximated by a linear function, with a transfer function incorporating the sensitivity to the oscillatory frequency and velocity. Linear models, could facilitate the use of stochastic based fatigue life estimates.

However, the application of linear models for use in stochastic or time domain models at high frequencies or relatively large turbulence intensities is arguable, given the non-linearities that were observed. Dynamic stall is likely to be an important consideration for turbines and drive the operational boundaries. This is of particular importance for turbines which operate near optimal power, as well as those which do not have a pitch actuating system. The dynamic loads and the point of flow reattachment has been shown here as being both frequency and amplitude dependent, and result in significant non-linear loads. The feasibility of an attenuation factor for these cases is also likely to be inappropriate.

Experimental testing is challenging and expensive, and blade developers are likely to also be interested in modelling these loads

numerically. Traditional analytical 2D oscillatory models which describe the response at the blade section level, appear to show promise for high frequency oscillations, particularly when flow separation is present. Semi-empirical dynamic stall models, such as the Beddoes–Leishman model employed in wind turbine analyses are likely to be useful, but challenging to validate. It is likely that these models may need to be tuned as to correctly model the movement of the separation point. For attached flow, dynamic inflow models are likely to be useful if the frequency is relatively low. Models such as that developed by Pitt and Peters (1981) can be incorporated in blade element-momentum type algorithms and account for the lag in the induced velocity following a change in rotor loading.

7. Conclusions

This study aimed to provide a quantitative assessment of the role of unsteadiness on the blade root out-of-plane bending moment. The experimental set-up, consisting of an auxiliary carriage system inducing planar oscillatory motion permitted the sensitivity of the bending moment response to various forcing conditions to be observed and analysed. For attached flow, the magnitude of the unsteady hydrodynamic contribution was found to be relatively small compared to the loads measured in steady flow. A phase lead was observed at low frequencies, and for which it is postulated that the dynamic inflow effects associated with circulation in the trailed wake dominates the shed wake circulation, and added mass. At higher frequencies the unsteady loads in phase with acceleration were, however, observed to be comparatively much smaller. At low tip-speed ratios, characteristics associated with flow separation were identified, for which a phase lag was observed in the attached flow. This suggests that the shed wake effects can become much more dominant. The relatively large loads experienced during dynamic stall, which were approximately 25% greater than that for steady flow, are likely to impose operational boundaries for tidal turbines.

The response to multi-frequency oscillatory motion was briefly considered. Reconstructing the multi-frequency response using both the steady flow measurements, and the single frequency response, was shown to offer a relatively good fit when the flow was attached, particularly for lower frequency combinations. This is promising for purposes of fatigue calculations. However, higher frequency cases exhibit substantial non-linearities, leading to significant underestimation of peak loads. Predicting the behaviour in these cases is likely to prove challenging.

Acknowledgements

This study has been conducted as part of a Ph.D. program and I.A. Milne acknowledges the financial assistance of the Bright Futures Top Achiever Doctoral Scholarship. The experimental equipment used in this study was built with the support of the UK EPSRC Grant EP/F062036/1 “Feasibility of an Innovative Methodology for Testing Marine Current Turbines in Unsteady Flow”. The authors acknowledge the Department of Naval Architecture and Marine Engineering at the University of Strathclyde for technical expertise and support. The guidance of Prof. J.M.R. Graham at Imperial College, London, is also greatly appreciated.

References

Bahaj, A.S., Batten, W.M.J., McCann, G., 2007a. Experimental verifications of numerical predictions for the hydrodynamic performance of horizontal axis marine current turbines. Renewable Energy 32, 2479–2490.

Bahaj, A.S., Molland, A.F., Chaplin, J.R., Batten, W.M.J., 2007b. Power and thrust measurements of marine current turbines under various hydrodynamic flow conditions in a cavitation tunnel and a towing tank. Renewable Energy 32, 407–426.

Barltrop, N., Varyani, K.S., Grant, A., Clelland, D., Xuan, P., 2006. Wave-current interactions in marine current turbines. Proc. Inst. Mech. Eng. Part M J. Eng. Marit. Environ. 220, 195–203.

Barnsley, M., Wellicome, J., 1992. Wind tunnel investigation of stall aerodynamics for a 1.0 m horizontal axis rotor. J. Wind Eng. Ind. Aerodyn. 39, 11–21.

Coleman, H.W., Steele, W.G., 2009. Experimental Validation and Uncertainty Analysis for Engineers, 3 edition John Wiley and Sons.

Connell, J.R., 1982. The spectrum of wind speed fluctuations encountered by a rotating blade of a wind energy conversion system. Solar Energy 29, 363–375.

Du, Z., Selig, M.S., 1998. A 3-d stall-delay model for horizontal axis wind turbine performance prediction. In: AIAA, Aerospace Sciences Meeting and Exhibit, 36th, and 1998 ASME Wind Energy Symposium, Reno, NV, United States, pp. 9–19.

Fraenkel, P., 2007. Marine current turbines: pioneering the development of marine kinetic energy converters. Proc. Inst. Mech. Eng. Part A: J. Power Energy 221, 159–169.

Galloway, P.W., Myers, L.E., Bahaj, A.S., 2010. Studies of a scale tidal turbine in close proximity to waves. In: Proceedings of the 3rd International Conference on Ocean Energy, Bilbao, Spain.

Hansen, M.O.L., 2008. Aerodynamics of Wind Turbines, 2 ed. Earthscan.

Hansen, M.H., Gaunna, M., Madsen, H.A., 2004. A Beddoes–Leishman Type Dynamic Stall Model in State-space and Indicial Formations. Technical Report R-1354. Riso National Laboratory, Roskilde, Denmark.

ITTC, 2006. Testing and Extrapolation Methods, General Density and Viscosity of Water 7.5-02-01-03.

ITTC, 2008a. Forces and moment Uncertainty Analysis, Example for Planar Motion Mechanism Test 7.5-02 06-04.

ITTC, 2008b. Testing and Extrapolation Methods, General Guidelines for Uncertainty Analysis in Resistance Towing Tank Tests 7.5-02-02-02.

ITTC, 2008c. Uncertainty Analysis Instrument Calibration 7.5-01-03-01.

Janiszewska, J.M., Reuss Ramsay, R., Hoffmann, M.J., Gregorek, G.M., 1996. Effects of Grit Roughness and Pitch Oscillations on the S814 Airfoil. Technical Report TP-422-8161. NREL.

Leishman, J., Beddoes, T., 1989. A semi-empirical model for dynamic stall. J. Am. Helicopter Soc. 34, 3–17.

Leishman, J.G., 2002. Challenges in modelling the unsteady aerodynamics of wind turbines. Wind Energy 5, 85–132.

Leishman, J.G., 2006. Principles of Helicopter Aerodynamics, second edition Cambridge University Press, Cambridge Aerospace.

Leishman, J.G., Beddoes, T.S., 1986. A generalized model for airfoil unsteady behaviour and dynamic stall using the indical method. In: Proceedings of the 42nd Annual Forum of the American Helicopter Society, Washington, DC, pp. 243–266.

Loewy, R.G., 1957. A two-dimensional approximation to the unsteady aerodynamics of rotary wings. J. Am. Helicopter Soc. 24, 81–92.

Maganga, F., Germain, G., King, J., Pinon, G., Rivoalen, E., 2010. Experimental study to determine flow characteristic effects on marine current turbine behaviour. IET Renewable Power Gener. 4, 498–509.

Marsh, G., 2009. Wave and tidal power—an emerging new market for composites. Reinf. Plast. 53, 20–24.

Milne, I.A., Sharma, R.N., Flay, R.G.J., Bickerton, S. Characteristics of the turbulence in the flow at a tidal-stream power site. Phil. Trans. R. Soc. A, 20120196, http://dx.doi.org/10.1098/rsta.2012.0196, in press.

Myers, L., Bahaj, A.S., 2006. Power output performance characteristics of a horizontal axis marine current turbine. Renewable Energy 31, 197–208.

Myers, L., Bahaj, A.S., 2007. Wake studies of a 1/30th scale horizontal axis marine current turbine. Ocean Eng. 34, 758–762. 0029-8018, http://dx.doi.org/10.1016/j.oceaneng.2006.04.013.

Pitt, L., Peters, D.A., 1981. Theoretical prediction of dynamic inflow derivatives. Vertica 5.

Rules for Classification and Construction, IV Industrial Services, Part 14 – Offshore Wind Energy, Guideline for the Certification of Ocean Energy Converters Part 1 Ocean Current Turbines, 2005. Germanischer Lloyd WindEnergie.

Shipley, D.E., Miller, M.S., Robinson, M.C., 1995. Dynamic stall occurrence on a horizontal axis wind turbine blade. In: Proceedings of the 1995 American Society of Mechanical Engineers (ASME) Energy Sources Technology Conference and Exhibition, Houston, TX, United States.

Theodorsen, T., 1935. General Theory of Aerodynamic Instability and the Mechanism of Flutter. Technical Report NACA Report 496.

Whelan, J.I., 2010. A Fluid Dynamic Study of Free-surface Proximity and Inertia Effects of Tidal Turbines. Ph.D. Thesis. Imperial College of Science, Technology and Medicine, Prince Consort Road, London.